THE JOURNAL OF PHYSICAL CHEMISTRY C
A JOURNAL OF THE AMERICAN CHEMICAL SOCIETY

pubs.acs.org/JPCC

Article

Electronic Densification and Stiffening of Diamond

Yan Wang,[†] Yongzhe Guo,[†] and Enlai Gao*

Cite This: *J. Phys. Chem. C* 2023, 127, 9931−9938

Read Online

ACCESS | Metrics & More | Article Recommendations | Supporting Information

ABSTRACT: Diamond, with a bulk modulus of 435 GPa, is the most incompressible natural material. Searching for ultra-incompressible materials with a bulk modulus significantly higher than diamond has attracted much attention. However, this search has been long questioned since it has not found incompressible materials significantly superior to diamond to date. From first-principles calculations, we here demonstrate that the density (4.34 g/cm^3) and the bulk modulus (645 GPa) of the electronically modified diamond can exceed 23% and 48% of the pristine diamond. Meanwhile, the tensile strength and strain-to-failure increase from 86 GPa and 13% for the pristine diamond to 242 GPa and 30% for the electronically modified diamond. These results indicate simultaneous stiffening, strengthening, and toughening of the diamond upon electronic modifications. Electronic structure analyses show that the ultrahigh density and mechanical performance of the electronically modified diamond are attributed to the shortening and stiffening of covalent bonds from the increase of bonding electron density.

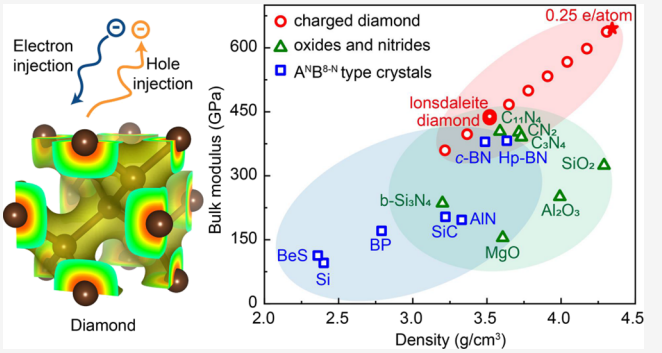

INTRODUCTION

Bulk modulus, defined as the ratio of volumetric stress to the volumetric strain, is a physical measure that characterizes the incompressibility of materials. High bulk modulus materials (e.g., diamond, the most incompressible natural crystal with a bulk modulus of 435 GPa) have been used in a wide range of industrial applications,[1−3] such as abrasives and cutting tools. Driven by the increasing industrial demand, considerable efforts have been devoted to searching for more incompressible materials.[4−6] Since the trial-and-error experimental approach is time-consuming, current approaches are mainly based on high-fidelity first-principles calculations, efficient empirical/semi-empirical formulae,[7−13] and high-throughput data-driven approaches such as machine learning and data mining.[4,5,14]

With the development of computational power, first principles provide a useful tool to predict the properties of a material based on its structure.[15] By using first-principles calculations, Swamy and Muddle[16] identified an ultrastiff cubic TiO_2. Wang et al.[17] found low-temperature phase transformation from graphite to sp^3 orthorhombic carbon that has a high bulk modulus comparable to that of the diamond. To predict material properties more efficiently, Kamran et al.[6] proposed semiempirical formulae for the bulk modulus of diamond-like and zinc-blende covalent crystals in terms of the bond length and ionicity fraction of the bonding. Li et al.[9,10] demonstrated that the bulk modulus essentially depends on the electronegativity and proposed a formula to predict the bulk modulus and hardness of crystalline materials. Furthermore, data-driven approaches have been developed to accelerate the discovery of ultra-incompressible materials, which discover numerous high bulk modulus materials from material databases. For example, Zeng et al.[4] screened out 50 materials with the largest predicted bulk moduli from 18,493 stable inorganic compounds, in which the highest bulk modulus is found as 401 GPa for Re_2C. The development of these approaches has driven the continuous discovery of new materials with a high bulk modulus, such as transition metal and transition-metal dioxides (e.g., 396 GPa for RuNF, 343 GPa for RuO_2, 382−476 GPa for Os, and 411 GPa for OsO_2).[18−20] More interestingly, it has been reported that C_3N_4 (451 GPa),[21] *c*-BN (376−404 GPa),[22,23] ReC (418−440 GPa),[24,25] and lonsdaleite (437 GPa)[26,27] have a bulk modulus rivaling that of the diamond. However, this search did not yield incompressible materials significantly superior to diamond to date. It has even been concluded that the bulk modulus for any material will not exceed 10−20% of diamond under ambient temperature and pressure.[28]

In addition to searching for new materials, structural modifications of existing materials can be used for higher performance.[29,30] For example, Huang et al.[31] synthesized nanotwinned diamond with unprecedented hardness through

Received: March 29, 2023
Revised: April 17, 2023
Published: May 11, 2023

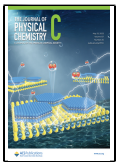

https://doi.org/10.1021/acs.jpcc.3c02079
J. Phys. Chem. C 2023, 127, 9931−9938

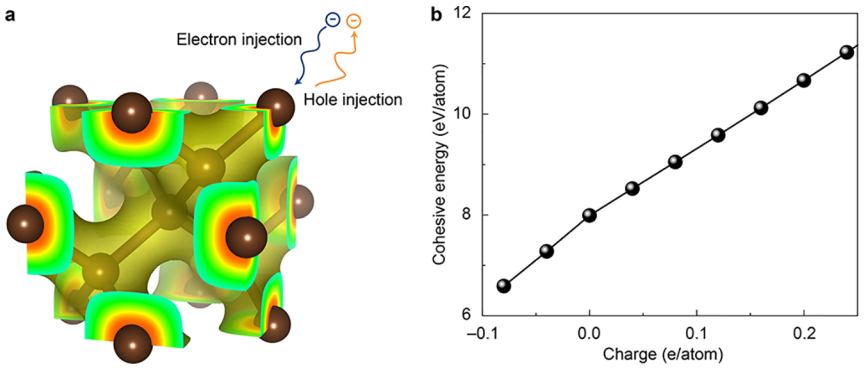

Figure 1. Structures and energies of the electronically modified diamond. (a) Illustration of charge injection into the diamond. (b) Cohesive energy of the diamond as a function of charge injection. Negative values of charge injection indicate electron injection into the diamond, while positive values indicate hole injection (depletion of the electron) into the diamond.

direct conversions of certain carbon precursors at high pressure and high temperature. Yue et al.[32] reported a hierarchically structured diamond composite with exceptional toughness. Under high pressures and temperatures, Xie et al.[33] have demonstrated that the bulk modulus of diamond can be improved to the maximum value of about 3200 GPa by first-principles calculations, which is attributed to the increase in atomic density and density of valence electrons. In addition to these structural modifications, it is still an open question whether there are more convenient approaches to enhance the performance of diamond. Fortunately, it has been found that linear atomic chains,[34] graphene,[35] graphene oxide,[36] phosphorene,[37] and Ti_2C MXene[38] upon charge injection exhibit extraordinary structural and mechanical responses. In 2012, Si et al.[39] reported that moderate charge injection of either electrons or holes can enhance the ideal strength of graphene by up to 17%. These results provide inspiration for modifying the electronic structure of diamond for higher performance.

In this work, we demonstrate that, upon electronic modification, the density, bulk modulus, tensile strength, and strain-to-failure of the diamond can be improved from 3.52 g/cm^3, 435 GPa, 86 GPa, and 13% to the maximum values of 4.34 g/cm^3, 645 GPa, 242 GPa, and 30%, respectively. These results indicate simultaneous stiffening, strengthening, and toughening of the diamond upon electronic modifications. Electronic structure analyses indicate that the shortening and stiffening of covalent bonds from the increase in bonding electron density account for the ultrahigh performance of the electronically modified diamond.

METHODS

First-principles calculations were performed under the framework of density functional theory using the Vienna Ab-Initio Simulation Package (VASP).[40] The Perdew−Burke−Ernzerhof (PBE) parameterization[41] of the generalized gradient approximation (GGA)[42] was adopted for the exchange-correlation functional. For comparison, calculations using the local density approximation (LDA) for the exchange-correlation functional were also performed. In the energy-minimized calculations, an energy cut-off of 520 eV and a *k*-point mesh with a density of over 30 Å (the product of each lattice constant and the corresponding number of *k*-points) were adopted.[43] All atomic positions and lattice parameters of the structures were optimized until all forces were less than 0.01 eV/Å. Injected charges (electrons and holes) were compensated using a background jellium to maintain charge neutrality in the computational cell. To be specific, the number of electrons was controlled by the keyword "NELECT" in VASP, which simulates the charge injection by adding or removing electrons to the structure with a compensating uniform charge background of the opposite sign. Such a jellium model has been found to well describe the structural, mechanical, and electronic properties of charged materials.[44−47] In ab initio molecular dynamics (AIMD) simulations, the energy cutoff of 400 eV is used for a balance between computational accuracy and cost. The temperature was controlled by using an Andersen thermostat.[48]

RESULTS AND DISCUSSION

Stabilities of the Electronically Modified Diamond. DFT calculations were used to investigate the structures and stabilities of the electronically modified diamond (Figure 1a). First, diamond structures upon different charge injections were structurally optimized, and thereafter, their elastic tensors were calculated using a strain−stress method.[49] The elastic tensors for diamond structures upon charge injection ranging from −0.08 to +0.25 e/atom are positive-definite, indicating that the Born elastic stability criteria are satisfied (Table S1). In the following text, only these elastically stable diamond structures were further investigated. Meanwhile, phonon calculations provide a criterion for quantifying structural stability. Our calculations do not find negative frequencies for diamond upon charge injections from −0.08 to +0.25 e/atom (Figure S1), which indicates their dynamic stabilities. Afterward, cohesive energy that provides a criterion for characterizing the thermal stability of materials was calculated (Figure 1b) The result shows that the cohesive energy for the diamond increases from 6.6 to 11.4 eV/atom as the charge injection increases from −0.08 to +0.25 e/atom, indicating the significant increase in the thermal stability of diamond upon hole injection compared with that of the pristine diamond with a cohesive energy of 8.0 eV/atom. Electron injection would excite electrons to higher energy states, while injected holes would induce electrons to lower energy states. These results account for the decreased and increased cohesive energies of the diamond upon electron and hole injections, respectively. Finally, ab initio molecular dynamics (AIMD) simulations were performed to explore the thermodynamic stabilities of the electronically modified diamond. These simulations were performed on a supercell of 64 atoms for 10 ps at 300 K, and the temperature was controlled by using an Andersen thermostat.[48] The evolution of temperature and system energy is gentle. As shown in

https://doi.org/10.1021/acs.jpcc.3c02079
J. Phys. Chem. C 2023, 127, 9931−9938

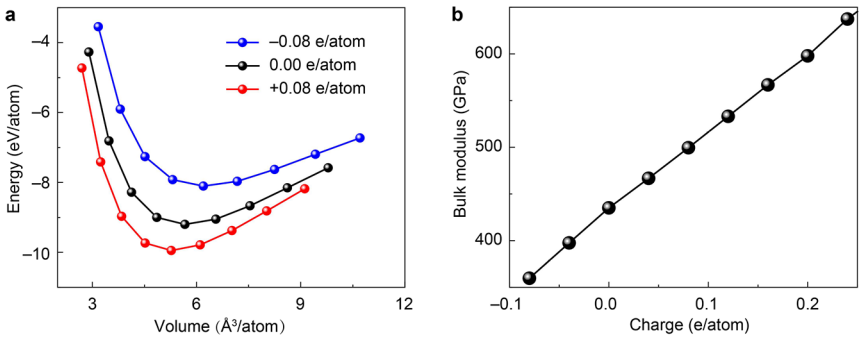

Figure 2. Incompressibility of the electronically modified diamond. (a) Energy as a function of volume change for the diamond upon charge injection of −0.08, 0.00, and +0.08 e/atom, respectively. (b) Bulk modulus for the diamond upon charge injection.

Movies S1 and S2, the electronically modified diamond upholds its structural integrity with only slight corrugation because of thermal fluctuations for the duration of the AIMD simulations. These results indicate the elastic, thermal, and thermodynamic stabilities of the electronically modified diamond upon charge injection ranging from −0.08 to +0.25 e/atom, which can be seen as the upper limit of charge doping in the computations.

Ultrahigh Density and Incompressibility of the Electronically Modified Diamond. To explore the incompressibility, we extracted the Hill average bulk modulus from the calculated elastic tensors of the electronically modified diamond. For comparison, DFT calculations at the local density approximation (LDA) and generalized gradient approximation (GGA) levels were performed. As shown in Figure S2a, the bulk moduli of the electronically modified diamond calculated using these two methods are in good agreement. Considering the accuracy, the following mechanical properties and the relevant structural analyses were calculated at the GGA level. We also performed calculations using computational cells of different sizes (primitive, unit, and supercells, Figure S2b), indicating that the calculated results are almost independent on the computational cell sizes. The below-reported results were calculated using a unit cell of the diamond.

The energy of the electronically modified diamond as a function of volume change shows that the energy changes more sharply as charge injection increases from negative to positive values (Figure 2a), signaling the increase in the bulk modulus. Furthermore, the bulk moduli of the electronically modified diamond were extracted from the calculated elastic tensors. The results show that the bulk moduli increase almost linearly as the charge injection increase from −0.08 to +0.25 e/atom (Figure 2b). The density and the bulk modulus are improved from 3.52 g/cm^3 and 435 GPa for the pristine diamond to the maximum values of 4.34 g/cm^3 and 645 GPa for the electronically modified diamond, indicating the ultrahigh-density and ultra-incompressibility of the electronically modified diamond. A literature survey shows that the highest value of bulk moduli of the electronically modified diamond is significantly superior to any known materials upon no charge injection (Figure 3). Furthermore, we used the same method to calculate the bulk moduli for typical ultra-incompressible materials (C_3N_4, BN, ReC, OsO_2, and lonsdaleite) upon charge injection. It was found (Figure S3) that the bulk modulus of the electronically modified diamond is also higher than these materials upon the same level of charge injection. These results indicate that the most

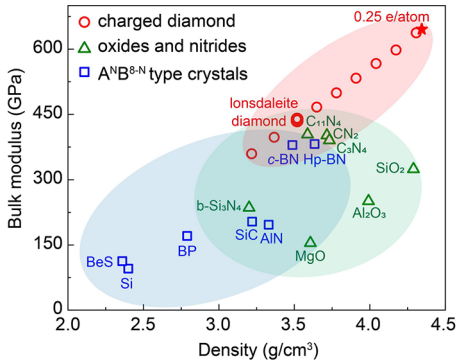

Figure 3. Comparison of bulk modulus and density of the electronically modified diamond with other highly incompressible materials. The raw data are provided in Table S2.

incompressible material under ambient temperature and pressure can be obtained through electronically modifying diamond. We also investigated the effect of defects (substitution and vacancy defects) on the densification and stiffening of diamond (Figure S4). Specifically, diamonds with substitution and vacancy defects were constructed from supercells of defect-free diamond with 32 atoms by replacing one carbon atom with one boron atom and one vacancy, respectively. Compared to defect-free diamond, the density and bulk modulus of defective diamonds also increase as the hole injection increases. These results indicate that the strategy of electronic densification and stiffening is also effective for defective diamonds despite the fact that the defects generally reduce the performance.

Meanwhile, the strength and toughness of materials are important for practical applications. We here probed such properties by performing uniaxial tensile tests on the electronically modified diamond along the highest Young's modulus direction (<111> direction). Like the bulk modulus, both the tensile strength and strain-to-failure increase as the charge injection increases from −0.08 to +0.25 e/atom (Figure 4). The tensile strength and strain-to-failure increase from 86 GPa and 13% for the pristine diamond to the maximum values of 242 GPa and 30% for the diamond upon hole injection of +0.25 e/atom. To our knowledge, no materials have both a higher strength and a higher strain-to-failure than those of the diamond upon the optimal charge injection. These above results demonstrate that electronic modifications can be used for the simultaneous stiffening, strengthening, and toughening of the diamond.

https://doi.org/10.1021/acs.jpcc.3c02079
J. Phys. Chem. C 2023, 127, 9931−9938

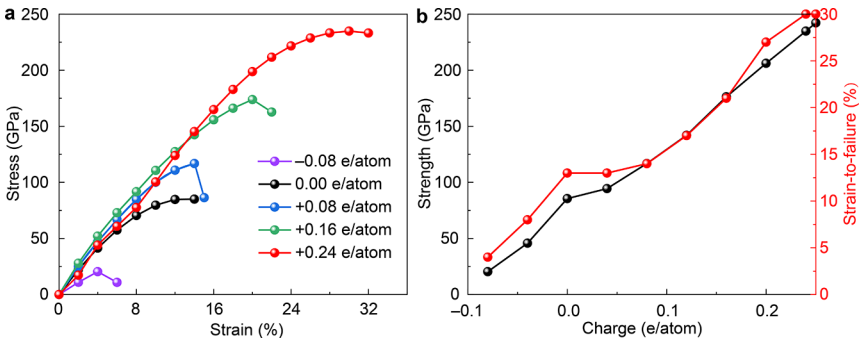

Figure 4. Uniaxial tensile behavior of the electronically modified diamond. (a) Tensile stress−strain curves for the diamond upon charge injection of −0.08, 0.00, +0.08, +0.16, and +0.24 e/atom. (b) Tensile strength and strain-to-failure of the electronically modified diamond in the highest Young's modulus direction (<111> direction).

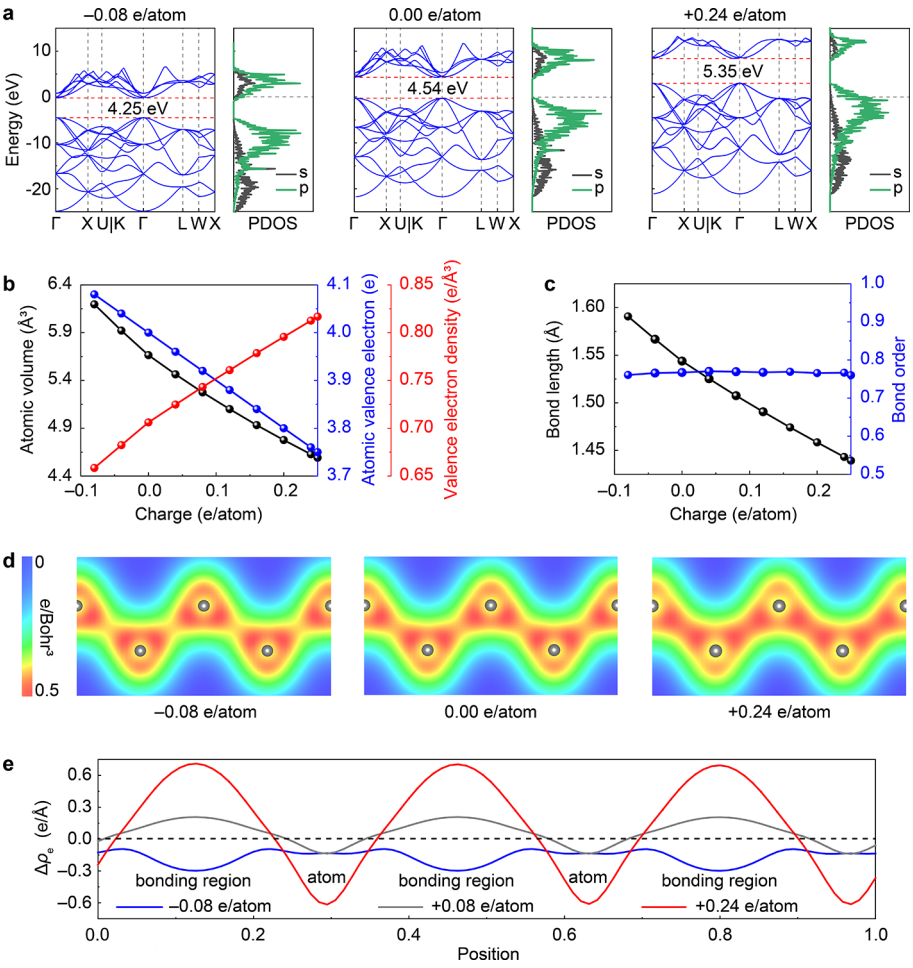

Figure 5. Mechanism analyses. (a) Band structures and projected densities of states (PDOS) of the electronically modified diamond. (b) Atomic volume, atomic valence electron, and valence electron density of the electronically modified diamond. (c) Bond length and bond order of the electronically modified diamond. (d) Charge density distribution of the electronically modified diamond with the iso-surface values of 0.5 e/Bohr^3. (e) Plane-averaged charge density difference along the highest modulus direction (<111> direction).

Mechanism Discussion. To understand the ultrahigh incompressibility of the electronically modified diamond, we first investigated the bonding state via band structures and projected densities of states (PDOS) (Figure 5a). The valence band of the pristine diamond consists of two regions showing high and low energies, which are mainly occupied by 2*p* and 2*s* states, respectively, whereas 2*p* states are dominant in the conduction band. Our DFT calculations at the PBE level show that the pristine diamond exhibits an indirect band gap of 4.54 eV, which is consistent with the previous DFT calculations at the same level.[50−52] The band gaps remain indirect for diamond upon charge injection. Notably, DFT calculations at the PBE level usually underestimated the values of the band gap due to the issue of exchange correlation. Hence, we performed additional DFT calculations at the HSE06 level.[53] The calculated band gap (5.52 eV) for the pristine diamond is also indirect and agree well with experimental values (5.47 eV[54] and 5.50 eV[55]), while the increased band gaps with the

https://doi.org/10.1021/acs.jpcc.3c02079
J. Phys. Chem. C 2023, 127, 9931−9938

charge injection is generally consistent with the calculations at the PBE level. As the injection increases, the conduction band minimum (CBM) increases more rapidly than the valence band maximum (VBM), which yields an increase in the band gap (Figures 5a and S5a). This increase in the band gap can account for the increase in the bulk modulus from this theoretical relation:[56] $\mu = pB + q$, where $\mu = E_g/\nu_b$ represents the excited energy density of chemical bonds, E_g is the band gap, ν_b is the average volume occupied by each bond, and p and q are constants. For charged diamonds, the determined relation is $\mu = 0.003B + 0.123$ (Figure S5b). To further explore the bonding mechanism, we performed crystal orbital Hamilton population (COHP) analyses[57,58] using the LOBSTER package[59,60] (Figure S5c). The integrated COHP (−ICOHP) that measures the covalent bond strength increases from 9.0 to 11.6 eV as the charge injection increases from −0.08 to +0.25 e/atom, indicating the significant strengthening of covalent bonds.

Next, we investigated the valence electron density to further understand the ultrahigh incompressibility of the electronically modified diamond. As shown in Figure 5b, although the atomic valence electron (valence electron per atom) of the electronically modified diamond decreases as charge injection increases, the atomic volume (volume per atom) decreases more sharply than the atomic valence electron, which results in an increase of valence electron density from 0.66 to 0.82 e·Å^{-3} as the charge injection increases from −0.08 to +0.25 e/atom. These results generally indicate that the improved valence electron density of the electronically modified diamond accounts for its enhanced incompressibility. To further understand the mechanical and structural responses of the diamond upon charge injection, the evolution of the bond length and the bond order was tracked (Figure 5c). The bond order that measures the number of chemical bonds between a pair of atoms was calculated based on a refinement of the density-derived electrostatic and chemical approach.[61] As the charge injection increases from −0.08 to +0.25 e/atom, the bond lengths of the diamond upon charge injection decrease from 1.59 to 1.44 Å, while the bond order remains almost a constant of 0.76 (Figure 5c), yielding a significant increase of bonding electron density. Such a significant increase in the bonding electron density also supports the significant strengthening of covalent bonds as discussed above.

Furthermore, electron density distribution shows that the electrons accumulate atop carbon atoms upon electron injection but accumulate in chemical bonds upon hole injection (Figure 5d and Movie S3). When the electrons accumulate atop carbon atoms upon electron injection, the Coulomb repulsion between atoms would increase, which accounts for the elongating of chemical bonds and enlarged atomic volume. When the electrons accumulate in chemical bonds upon hole injection, the bonding electron density would increase, which accounts for the shortening of chemical bonds and reduced atomic volume. To quantify the electron density distribution, we calculated the plane-averaged charge density difference[62] along the highest modulus direction (<111> direction), $\Delta\rho_e = \rho_c - \rho_0$, where ρ_c is the plane-average charge density upon charge injection and ρ_0 is the plane-average charge density without charge injection. The positive and negative values of $\Delta\rho_e$ in bonding regions indicate the increase and decrease in bonding electron density for the hole and electron-injected diamond structures, respectively (Figure 5e). The increase in the bonding electron density of the diamond upon hole injection is attributed to the reduced atomic volume and accumulated electrons in chemical bonds, while the decrease in bonding electron density of the diamond upon electron injection is attributed to the increased atomic volume and accumulated electrons atop carbon atoms. Despite the fact that Figure 5b has shown that the valence electron density of the electronically modified diamond increases as the charge injection increases from −0.08 to +0.25 e/atom, Figure 5c further demonstrates that the increase in bonding electron density is more important. To summarize, these above-mentioned results indicate that the ultrahigh mechanical performance of the diamond upon hole injection is attributed to the shortening and stiffening of covalent bonds that result from the increase of bonding electron density.

Additional Remarks on the Fabrication and Application of the Electronically Modified Diamond. The fabrication of the electronically modified diamond provides an enormous challenge. The attractive approaches are to modify the electronic structure by applying a gate voltage or by doping impurities.[63] For charge injection by applying a gate voltage, thin diamonds are favorable for high doping levels. Fortunately, nanodiamonds, such as diamane[64] and diamond nanothreads,[65−67] have been successfully fabricated. For charge injection by doping impurities, the doping-induced modification on the electronic structures is nonuniform, which can not ensure an increase in the bulk modulus. Hence, the challenge for this approach is to find effective doping manners, such as doping elements, sites, and concentrations.

The doping level is of central importance in these approaches. A literature survey shows that the highest experimental accessible doping level increases as the approaches develop. In 2008, Das et al.[68] reported the highest doping level of 5×10^{13} cm^{-2} (equivalent to 0.013 e/atom) for graphene transistors in the solid polymer electrolyte gate. In 2010, Efetov and Kim[69] demonstrated that the electron and hole doping levels of 4×10^{14} cm^{-2} (equivalent to 0.11 e/atom) for graphene can be accessed by employing an electrolytic gate. In 2012, Khrapach et al.[70] demonstrated a doping level of 9×10^{14} cm^{-2} (equivalent to 0.24 e/atom) for graphene by polyatomic ($FeCl_3$) intercalation. In 2012, Ye et al.[71] reported a high doping level of 1×10^{15} cm^{-2} (equivalent to 0.29 e/atom) for MoS_2 by monoatomic (Li, Na, and K) intercalation. In 2014, Bao et al.[72] demonstrated a high doping level of 3.5×10^{22} cm^{-3} (equivalent to 0.25 e/atom) for LiC_6 (Li-intercalated ultrathin graphite). In summary, the experimental accessible doping levels for 2D and 3D materials are 1×10^{15} cm^{-2} (equivalent to 0.29 e/atom)[71] and 3.5×10^{22} cm^{-3} (equivalent to 0.25 e/atom),[72] respectively. In our calculations, the highest doping level for diamond maintaining enough structural integrity is 0.25 e/atom. We hope that these calculations at the highest possible doping level can provide guidelines for future experimental studies.

The above results show that the electronically modified diamond has ultrahigh stiffness, strength, and toughness. Hence, a few suggestions for the electronically modified diamond applications are made, including cutting tools and protective coatings. When used as a cutting tool, the electronically modified diamond is expected to cut any material, even the pristine diamond, since it has higher stiffness, strength, and toughness than any raw material. When used as protective coatings, the electronically modified diamond is expected to provide active protection and long

https://doi.org/10.1021/acs.jpcc.3c02079
J. Phys. Chem. C 2023, 127, 9931−9938

service life since the enhanced mechanical performance can be activated or deactivated according to practical needs.

CONCLUSIONS

In summary, we computationally demonstrate that the diamond exhibits ultrahigh density and incompressibility while maintaining enough structural integrity under a certain amount of charge injection. The bulk modulus of the electronically modified diamond can increase by 48% compared with the pristine diamond, making the incompressibility of the electronically modified diamond significantly superior to any known materials upon no charge injection. Our calculations further found that, at the same doping level, the bulk modulus of the diamond is also higher than typical ultra-incompressible materials (C_3N_4, BN, ReC, OsO_2, and lonsdaleite). Furthermore, the tensile strength and strain-to-failure of the diamond can increase by 181% and 131% upon the optimal charge injection, respectively. These results indicate that charge engineering can be used for stiffening, strengthening, and toughening the diamond. Structural analyses indicate that the ultrahigh mechanical performance of the electronically modified diamond results from the shortening and stiffening of covalent bonds from the increase of bonding electron density. Finally, the possible fabrication and application of the electronically modified diamond are discussed.

ASSOCIATED CONTENT

Supporting Information

The Supporting Information is available free of charge at https://pubs.acs.org/doi/10.1021/acs.jpcc.3c02079.

Phonon dispersion of the electronically modified diamond; comparison of the bulk moduli calculated by different methods and different crystal sizes; bulk moduli of the electronically modified diamond as compared with other typical ultra-incompressible materials upon charge injection; performance of defective diamonds as compared with those of defect-free diamond; mechanism analyses of the electronic structures; and raw data of calculations and relevant literature (PDF)

AIMD simulation of the diamond upon charge injection of −0.08 e/atom (MP4)

AIMD simulation of the diamond upon charge injection of +0.25 e/atom (MP4)

Electron density redistribution for the diamond upon charge injection (MP4)

AUTHOR INFORMATION

Corresponding Author

Enlai Gao − *Department of Engineering Mechanics, School of Civil Engineering, Wuhan University, Wuhan, Hubei 430072, China;* orcid.org/0000-0003-1960-0260; Email: enlaigao@whu.edu.cn

Authors

Yan Wang − *Department of Engineering Mechanics, School of Civil Engineering, Wuhan University, Wuhan, Hubei 430072, China*

Yongzhe Guo − *Department of Engineering Mechanics, School of Civil Engineering, Wuhan University, Wuhan, Hubei 430072, China*

Complete contact information is available at: https://pubs.acs.org/10.1021/acs.jpcc.3c02079

Author Contributions

†Y.W. and Y.G. contribute equally.

Notes

The authors declare no competing financial interest.

ACKNOWLEDGMENTS

This work was supported by the National Natural Science Foundation of China (12172261). The numerical calculations in this work have been performed on a supercomputing system in the Supercomputing Center of Wuhan University.

REFERENCES

(1) Ward, A.; Broido, D. A.; Stewart, D. A.; Deinzer, G. *Ab initio* theory of the lattice thermal conductivity in diamond. *Phys. Rev. B* **2009**, *80*, No. 125203.

(2) Abyzov, A. M.; Kidalov, S. V.; Shakhov, F. M. High thermal conductivity composite of diamond particles with tungsten coating in a copper matrix for heat sink application. *Appl. Therm. Eng.* **2012**, *48*, 72−80.

(3) Kaner, R. B.; Gilman, J. J.; Tolbert, S. H. Designing superhard materials. *Science* **2005**, *308*, 1268−1269.

(4) Zeng, S.; Li, G.; Zhao, Y.; Wang, R.; Ni, J. Machine learning-aided design of materials with target elastic properties. *J. Phys. Chem. C* **2019**, *123*, 5042−5047.

(5) Mansouri Tehrani, A.; Oliynyk, A. O.; Parry, M.; Rizvi, Z.; Couper, S.; Lin, F.; Miyagi, L.; Sparks, T. D.; Brgoch, J. Machine learning directed search for ultraincompressible, superhard materials. *J. Am. Chem. Soc.* **2018**, *140*, 9844−9853.

(6) Kamran, S.; Chen, K.; Chen, L. Semiempirical formulae for elastic moduli and brittleness of diamondlike and zinc-blende covalent crystals. *Phys. Rev. B* **2008**, *77*, No. 094109.

(7) Hopfield, J. J. The physics of bonding: Bonds and bands in semiconductors. *Science* **1974**, *183*, 403−404.

(8) Cohen, M. L. Calculation of bulk moduli of diamond and zinc-blende solids. *Phys. Rev. B* **1985**, *32*, 7988−7991.

(9) Li, K.; Wang, X.; Zhang, F.; Xue, D. Electronegativity identification of novel superhard materials. *Phys. Rev. Lett.* **2008**, *100*, No. 235504.

(10) Li, K.; Ding, Z.; Xue, D. Electronegativity-related bulk moduli of crystal materials. *Phys. Status Solidi B* **2011**, *248*, 1227−1236.

(11) Mattsson, A. E.; Schultz, P. A.; Desjarlais, M. P.; Mattsson, T. R.; Leung, K. Designing meaningful density functional theory calculations in materials science—a primer. *Modell. Simul. Mater. Sci. Eng.* **2005**, *13*, R1−R31.

(12) Ravindran, P.; Fast, L.; Korzhavyi, P. A.; Johansson, B.; Wills, J.; Eriksson, O. Density functional theory for calculation of elastic properties of orthorhombic crystals: Application to $TiSi_2$. *J. Appl. Phys.* **1998**, *84*, 4891−4904.

(13) Chen, X.-Q.; Niu, H.; Franchini, C.; Li, D.; Li, Y. Hardness of T-carbon: Density functional theory calculations. *Phys. Rev. B* **2011**, *84*, No. 121405.

(14) Shao, Q.; Li, R.; Yue, Z.; Wang, Y.; Gao, E. Data-driven discovery and understanding of ultrahigh-modulus crystals. *Chem. Mater.* **2021**, *33*, 1276−1284.

(15) Jain, A.; Ong, S. P.; Hautier, G.; Chen, W.; Richards, W. D.; Dacek, S.; Cholia, S.; Gunter, D.; Skinner, D.; Ceder, G.; Persson, K. A. The materials project: A materials genome approach to accelerating materials innovation. *APL Mater.* **2013**, *1*, No. 011002.

(16) Swamy, V.; Muddle, B. C. Ultrastiff cubic TiO_2 identified via first-principles calculations. *Phys. Rev. Lett.* **2007**, *98*, No. 035502.

(17) Wang, J. T.; Chen, C.; Kawazoe, Y. Low-temperature phase transformation from graphite to sp^3 orthorhombic carbon. *Phys. Rev. Lett.* **2011**, *106*, No. 075501.

(18) Gerward, L.; Staun Olsen, J.; Petit, L.; Vaitheeswaran, G.; Kanchana, V.; Svane, A. Bulk modulus of CeO_2 and PrO_2—An

experimental and theoretical study. *J. Alloys Compd.* **2005**, *400*, 56−61.
(19) Lundin, U.; Fast, L.; Nordström, L.; Johansson, B.; Wills, J. M.; Eriksson, O. Transition-metal dioxides with a bulk modulus comparable to diamond. *Phys. Rev. B* **1998**, *57*, 4979−4982.
(20) Sahu, B. R.; Kleinman, L. Osmium is not harder than diamond. *Phys. Rev. B* **2005**, *72*, No. 113106.
(21) Teter, D. M.; Hemley, R. J. Low-compressibility carbon nitrides. *Science* **1996**, *271*, 53−55.
(22) Yao, H.; Ouyang, L.; Ching, W.-Y. Ab initio calculation of elastic constants of ceramic crystals. *J. Am. Ceram. Soc.* **2007**, *90*, 3194−3204.
(23) Zhang, R. F.; Veprek, S.; Argon, A. S. Anisotropic ideal strengths and chemical bonding of wurtzite BN in comparison to zincblende BN. *Phys. Rev. B* **2008**, *77*, No. 172103.
(24) Zhang, X.; Chen, Z.; Fan, C.; Ma, M.; Jing, Q.; Liu, R. Supreme shear modulus predicted in the monocarbide system: The $Re_xW_{1-x}C$ alloy. *Phys. Status Solidi - Rapid Res. Lett.* **2009**, *3*, 299−301.
(25) Chen, Z.; Gu, M.; Sun, C. Q.; Zhang, X.; Liu, R. Ultrastiff carbides uncovered in first principles. *Appl. Phys. Lett.* **2007**, *91*, No. 061905.
(26) Qingkun, L.; Yi, S.; Zhiyuan, L.; Yu, Z. Lonsdaleite — a material stronger and stiffer than diamond. *Scr. Mater.* **2011**, *65*, 229−232.
(27) Kulnitskiy, B.; Perezhogin, I.; Dubitsky, G.; Blank, V. Polytypes and twins in the diamond−lonsdaleite system formed by high-pressure and high-temperature treatment of graphite. *Acta Crystallogr. B* **2013**, *69*, 474−479.
(28) Brazhkin, V. V.; Solozhenko, V. L. Myths about new ultrahard phases: Why materials that are significantly superior to diamond in elastic moduli and hardness are impossible. *J. Appl. Phys.* **2019**, *125*, 130901.
(29) Xiao, J.; Wen, B.; Xu, B.; Zhang, X.; Wang, Y.; Tian, Y. Intersectional nanotwinned diamond—the hardest polycrystalline diamond by design. *npj Comput. Mater.* **2020**, *6*, 119.
(30) Wen, B.; Xu, B.; Wang, Y.; Gao, G.; Zhou, X.-F.; Zhao, Z.; Tian, Y. Continuous strengthening in nanotwinned diamond. *npj Comput. Mater.* **2019**, *5*, 117.
(31) Huang, Q.; Yu, D.; Xu, B.; Hu, W.; Ma, Y.; Wang, Y.; Zhao, Z.; Wen, B.; He, J.; Liu, Z.; Tian, Y. Nanotwinned diamond with unprecedented hardness and stability. *Nature* **2014**, *510*, 250−253.
(32) Yue, Y.; Gao, Y.; Hu, W.; Xu, B.; Wang, J.; Zhang, X.; Zhang, Q.; Wang, Y.; Ge, B.; Yang, Z.; Li, Z.; et al. Hierarchically structured diamond composite with exceptional toughness. *Nature* **2020**, *582*, 370−374.
(33) Xie, J.; Chen, S. P.; Tse, J. S.; Gironcoli, S.; Baroni, S. High-pressure thermal expansion, bulk modulus, and phonon structure of diamond. *Phys. Rev. B* **1999**, *60*, 9444−9449.
(34) Gao, E.; Guo, Y.; Wang, Z.; Nielsen, S. O.; Baughman, R. H. The strongest and toughest predicted materials: Linear atomic chains without a peierls instability. *Matter* **2022**, *5*, 1192−1203.
(35) Rogers, G. W.; Liu, J. Z. Graphene actuators: Quantum-mechanical and electrostatic double-layer effects. *J. Am. Chem. Soc.* **2011**, *133*, 10858−10863.
(36) Rogers, G. W.; Liu, J. Z. Monolayer graphene oxide as a building block for artificial muscles. *Appl. Phys. Lett.* **2013**, *102*, No. 021903.
(37) Wu, B.; Deng, H.-X.; Jia, X.; Shui, L.; Gao, E.; Liu, Z. High-performance phosphorene electromechanical actuators. *npj Comput. Mater.* **2020**, *6*, 27.
(38) Wu, B.; Cai, X.; Shui, L.; Gao, E.; Liu, Z. Extraordinary electromechanical actuation of Ti_2C MXene. *J. Phys. Chem. C* **2021**, *125*, 1060−1068.
(39) Si, C.; Duan, W.; Liu, Z.; Liu, F. Electronic strengthening of graphene by charge doping. *Phys. Rev. Lett.* **2012**, *109*, No. 226802.
(40) Kresse, G.; Furthmüller, J. Efficiency of ab-initio total energy calculations for metals and semiconductors using a plane-wave basis set. *Comput. Mater. Sci.* **1996**, *6*, 15−50.
(41) Perdew, J. P.; Burke, K.; Ernzerhof, M. Generalized gradient approximation made simple. *Phys. Rev. Lett.* **1996**, *77*, 3865−3868.
(42) Filippi, C.; Singh, D. J.; Umrigar, C. J. All-electron local-density and generalized-gradient calculations of the structural properties of semiconductors. *Phys. Rev. B* **1994**, *50*, 14947.
(43) Monkhorst, H. J.; Pack, J. D. Special points for Brillouin-zone integrations. *Phys. Rev. B* **1976**, *13*, 5188.
(44) Xu, Y.; Zhou, J.; Dong, J. Infrared absorption spectra of few-layer graphenes studied by first principles calculations. *Phys. Lett. A* **2010**, *374*, 796−800.
(45) Lang, N. D.; Kohn, W. Surface-dipole barriers in simple metals. *Phys. Rev. B* **1973**, *8*, 6010−6012.
(46) Swift, D. C.; Lockard, T.; Hamel, S.; Wu, C. J.; Benedict, L. X.; Sterne, P. A. Atom-in-jellium predictions of the shear modulus at high pressure. *Phys. Rev. B* **2022**, *105*, No. 024110.
(47) Perdew, J. P.; Tran, H. Q.; Smith, E. D. Stabilized jellium: Structureless pseudopotential model for the cohesive and surface properties of metals. *Phys. Rev. B* **1990**, *42*, 11627−11636.
(48) Andersen, H. C. Molecular dynamics simulations at constant pressure and/or temperature. *J. Chem. Phys.* **1980**, *72*, 2384−2393.
(49) Le Page, Y.; Saxe, P. Symmetry-general least-squares extraction of elastic data for strained materials from *ab initio* calculations of stress. *Phys. Rev. B* **2002**, *65*, No. 104104.
(50) Ullah, M.; Ahmed, E.; Hussain, F.; Rana, A. M.; Raza, R. Electrical conductivity enhancement by boron-doping in diamond using first principle calculations. *Appl. Surf. Sci.* **2015**, *334*, 40−44.
(51) Czelej, K.; Śpiewak, P.; Kurzydłowski, K. J. Electronic structure and N-type doping in diamond from first principles. *MRS Adv.* **2016**, *1*, 1093−1098.
(52) Deák, P.; Aradi, B.; Frauenheim, T.; Janzén, E.; Gali, A. Accurate defect levels obtained from the HSE06 range-separated hybrid functional. *Phys. Rev. B* **2010**, *81*, No. 153203.
(53) Krukau, A. V.; Vydrov, O. A.; Izmaylov, A. F.; Scuseria, G. E. Influence of the exchange screening parameter on the performance of screened hybrid functionals. *J. Chem. Phys.* **2006**, *125*, 224106.
(54) Clark, C. D.; Dean, P. J.; Harris, P. V. Intrinsic edge absorption in diamond. *Proc. R. Soc. Lond. A Math. Phys. Sci.* **1964**, *277*, 312−329.
(55) Kalish, R. Diamond as a unique high-tech electronic material: Difficulties and prospects. *J. Phys. D: Appl. Phys.* **2007**, *40*, 6467−6478.
(56) Li, K.; Kang, C.; Xue, D. Relationship between band gap and bulk modulus of semiconductor materials. *Mater. Focus* **2012**, *1*, 88−92.
(57) Dronskowski, R.; Blöchl, P. E. Crystal orbital Hamilton populations (COHP): Energy-resolved visualization of chemical bonding in solids based on density-functional calculations. *J. Phys. Chem.* **1993**, *97*, 8617−8624.
(58) Deringer, V. L.; Tchougréeff, A. L.; Dronskowski, R. Crystal orbital Hamilton population (COHP) analysis as projected from plane-wave basis sets. *J. Phys. Chem. A* **2011**, *115*, 5461−5466.
(59) Maintz, S.; Deringer, V. L.; Tchougréeff, A. L.; Dronskowski, R. Analytic projection from plane-wave and PAW wavefunctions and application to chemical-bonding analysis in solids. *J. Comput. Chem.* **2013**, *34*, 2557−2567.
(60) Maintz, S.; Deringer, V. L.; Tchougréeff, A. L.; Dronskowski, R. LOBSTER: A tool to extract chemical bonding from plane-wave based DFT. *J. Comput. Chem.* **2016**, *37*, 1030−1035.
(61) Manz, T. A. Introducing DDEC6 atomic population analysis: Part 3. Comprehensive method to compute bond orders. *RSC Adv.* **2017**, *7*, 45552−45581.
(62) Li, X.-H.; Wang, B.-J.; Cai, X.-L.; Yu, W.-Y.; Zhu, Y.-Y.; Li, F.-Y.; Fan, R.-X.; Zhang, Y.-S.; Ke, S.-H. Strain-tunable electronic properties and band alignments in $GaTe/C_2N$ heterostructure: A first-principles calculation. *Nanoscale Res. Lett.* **2018**, *13*, 300.
(63) Wan, J.; Lacey, S. D.; Dai, J.; Bao, W.; Fuhrer, M. S.; Hu, L. Tuning two-dimensional nanomaterials by intercalation: Materials, properties and applications. *Chem. Soc. Rev.* **2016**, *45*, 6742−6765.
(64) Wort, C. J. H.; Balmer, R. S. Diamond as an electronic material. *Mater. Today* **2008**, *11*, 22−28.

https://doi.org/10.1021/acs.jpcc.3c02079
J. Phys. Chem. C 2023, 127, 9931−9938

(65) Roman, R. E.; Kwan, K.; Cranford, S. W. Mechanical properties and defect sensitivity of diamond nanothreads. *Nano Lett.* **2015**, *15*, 1585−1590.
(66) Zheng, Z.; Zhan, H.; Nie, Y.; Xu, X.; Qi, D.; Gu, Y. Single layer diamond — A new ultrathin 2D carbon nanostructure for mechanical resonator. *Carbon* **2020**, *161*, 809−815.
(67) Zhan, H.; Zhang, G.; Tan, V. B. C.; Gu, Y. The best features of diamond nanothread for nanofibre applications. *Nat. Commun.* **2017**, *8*, 14863.
(68) Das, A.; Pisana, S.; Chakraborty, B.; Piscanec, S.; Saha, S. K.; Waghmare, U. V.; Novoselov, K. S.; Krishnamurthy, H. R.; Geim, A. K.; Ferrari, A. C.; et al. Monitoring dopants by Raman scattering in an electrochemically top-gated graphene transistor. *Nat. Nanotechnol.* **2008**, *3*, 210−215.
(69) Efetov, D. K.; Kim, P. Controlling electron-phonon interactions in graphene at ultrahigh carrier densities. *Phys. Rev. Lett.* **2010**, *105*, No. 256805.
(70) Khrapach, I.; Withers, F.; Bointon, T. H.; Polyushkin, D. K.; Barnes, W. L.; Russo, S.; Craciun, M. F. Novel highly conductive and transparent graphene-based conductors. *Adv. Mater.* **2012**, *24*, 2844−2849.
(71) Ye, J. T.; Zhang, Y. J.; Akashi, R.; Bahramy, M. S.; Arita, R.; Iwasa, Y. Superconducting dome in a gate-tuned band insulator. *Science* **2012**, *338*, 1193−1196.
(72) Bao, W.; Wan, J.; Han, X.; Cai, X.; Zhu, H.; Kim, D.; Ma, D.; Xu, Y.; Munday, J. N.; Drew, H. D.; et al. Approaching the limits of transparency and conductivity in graphitic materials through lithium intercalation. *Nat. Commun.* **2014**, *5*, 4224.

https://doi.org/10.1021/acs.jpcc.3c02079
J. Phys. Chem. C 2023, 127, 9931−9938

Supporting Information

Electronic Densification and Stiffening of Diamond

Yan Wang,[§] Yongzhe Guo,[§] and Enlai Gao[*]

Department of Engineering Mechanics, School of Civil Engineering, Wuhan University, Wuhan, Hubei 430072, China.

[*]Corresponding author. Email: enlaigao@whu.edu.cn

This supporting information contains

(1) Figures S1-S5.

(2) Tables S1-S2.

(3) Movies S1-S3.

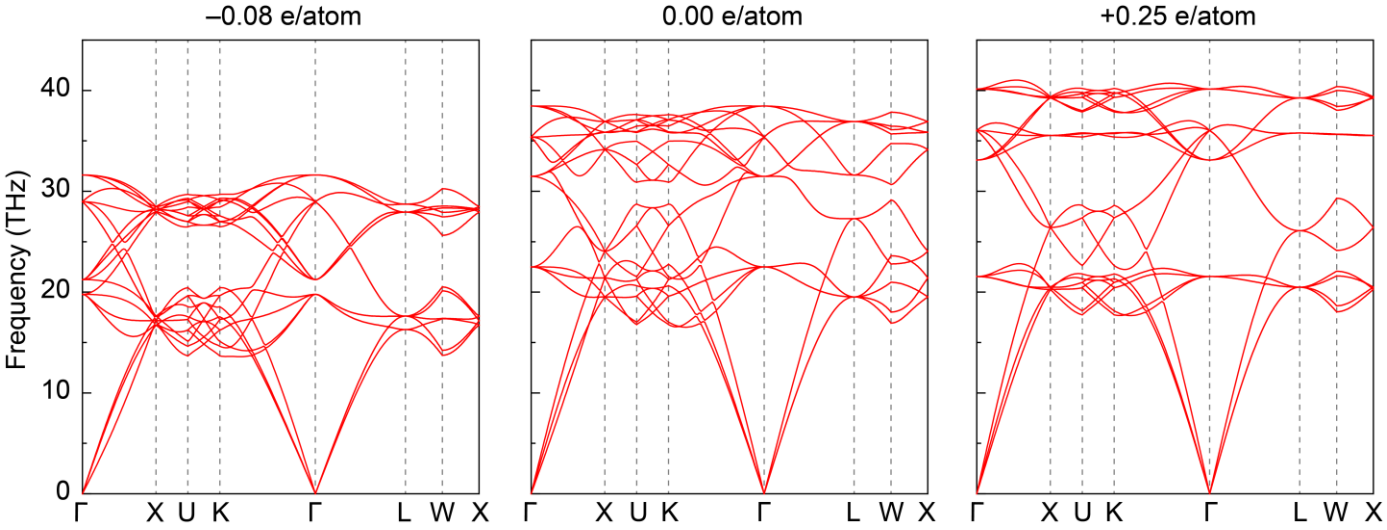

Fig. S1. Phonon dispersion of the electronically modified diamond upon charge injection of ¬0.08, 0.00, and +0.25 e/atom, respectively.

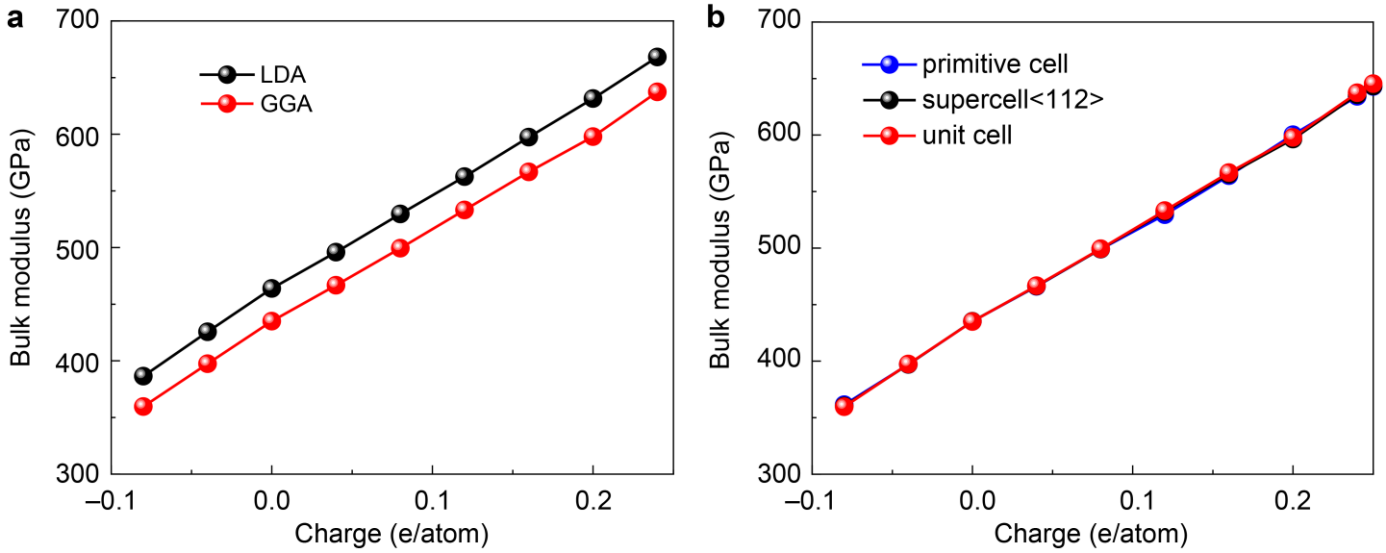

Fig. S2. Comparison of the bulk moduli calculated by different methods and different crystal sizes. (a) The bulk moduli are calculated at the local density approximation (LDA) and the generalized gradient approximation (GGA) levels. (b) The bulk moduli are calculated with different sizes at the GGA level.

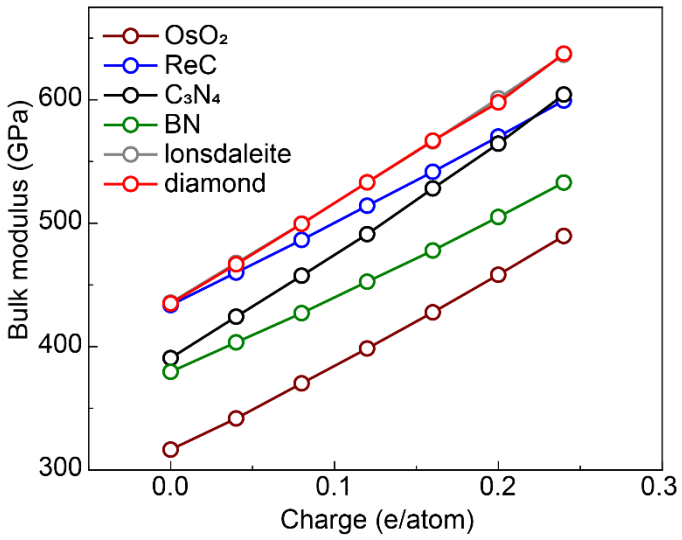

Fig. S3. Bulk moduli of the electronically modified diamond as compared with other typical ultra-incompressible materials upon charge injection.

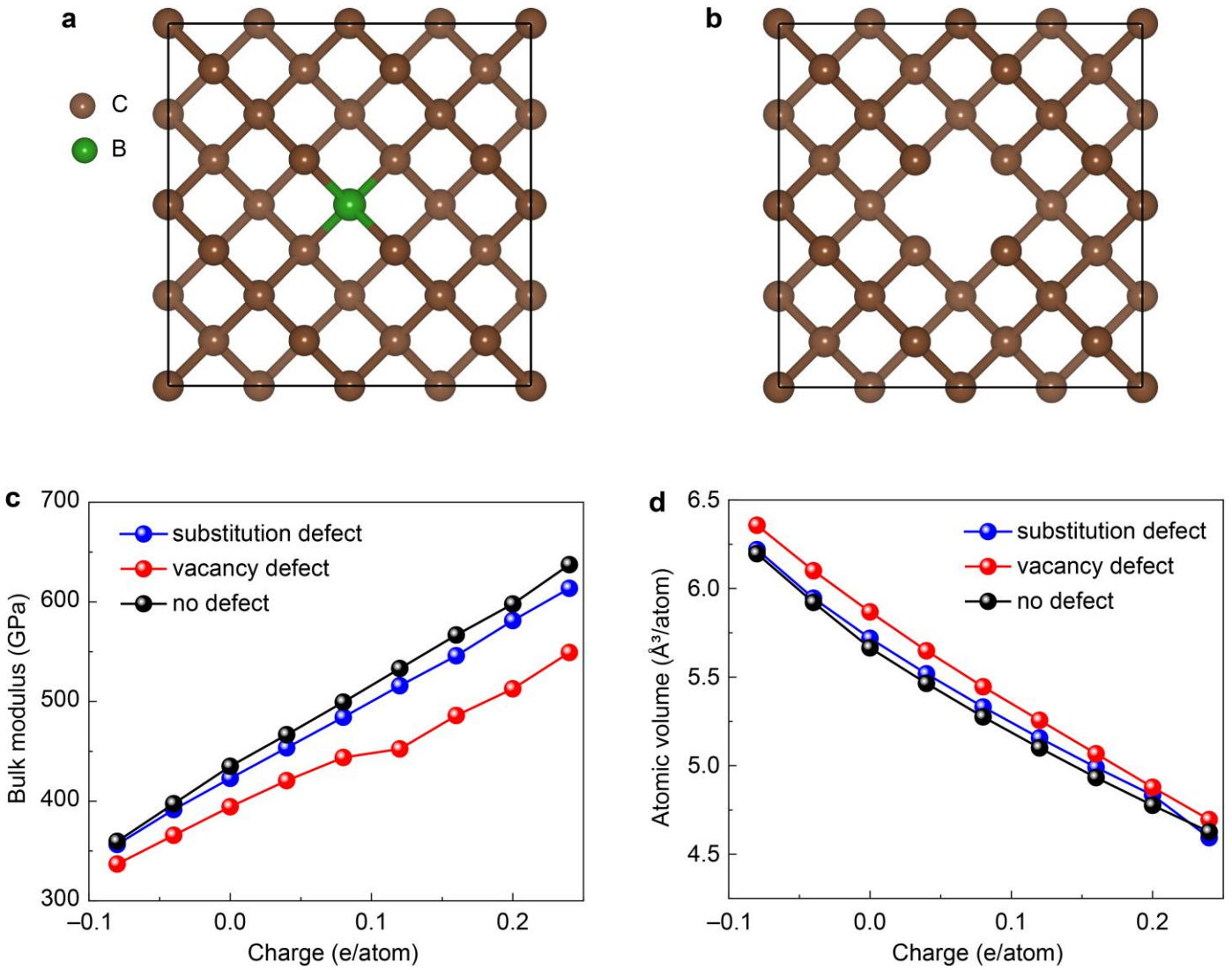

Fig. S4. Diamonds with (a) boron substitution and (b) vacancy defects. (c) Bulk modulus and (d) atomic volume of defective diamonds as compared with those of defect-free diamond.

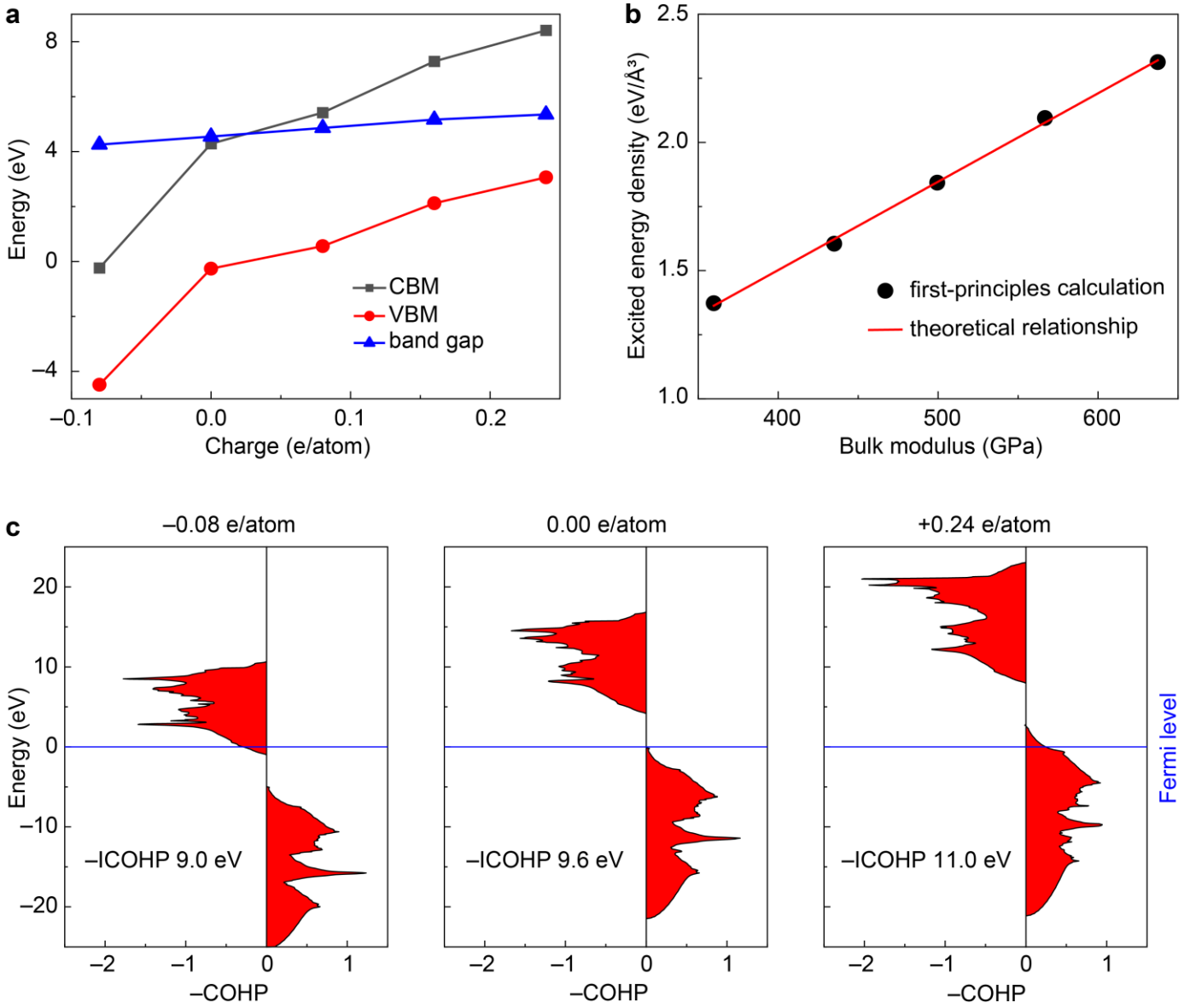

Fig. S5. Mechanism analyses of the electronic structures. (a) Valence band maximum (VBM), conduction band minimum (CBM), and band gap of the electronically modified diamond. (b) Linear relation between the excited energy density and the bulk modulus. (c) Crystal orbital Hamilton population (COHP) of the electronically modified diamond, where bonding interactions were plotted to the right, antibonding ones to the left.

Table. S1. Bulk modulus (B), tensile strength (σ_s) and strain to failure (ε_s) in the highest Young's modulus direction, and minimum eigenvalue (λ_{min}) calculated at the local density approximation (LDA) and the generalized gradient approximation (GGA) levels, respectively.

Charge (e/atom)	B (GPa)		σ_s (GPa)	ε_s	λ_{min} (GPa)	
	GGA	LDA			GGA	LDA
–0.08	359.7	386.5	20.4	0.04	231.7	246.8
–0.04	397.5	425.6	45.8	0.08	170.8	159.6
0	435.0	463.9	85.5	0.13	566.5	589.8
+0.04	466.7	495.9	94.4	0.13	598.7	620.8
+0.08	499.5	529.7	116.8	0.14	566.4	532.5
+0.12	533.1	562.6	142.0	0.17	555.4	562.8
+0.16	566.8	597.5	176.3	0.21	581.5	589.2
+0.20	597.9	631.5	206.1	0.27	468.2	423.4
+0.24	637.4	668.2	234.8	0.30	735.7	753.7
+0.25	645.4	681.7	242.2	0.30	385.9	312.0
+0.26					–105.9	–76.3

Table. S2. Density (ρ), volume (V) and bulk modulus (B) of the electronically modified diamond as compared with other highly incompressible materials.

Materials	ρ (g·cm^{-3})	V (Å ^{3})	B (GPa)	Refs
Diamond*	4.3	36.73	645	This work
Diamond	3.5	45.32	435	This work
Lonsdaleite	3.5	45.42	436	This work
Si	2.4	155.81	96	[1]
C_3N_4	3.7	40.98	391	This work
$C_{11}N_4$	3.6	87.12	404	This work
CN_2	3.7	71.58	402	This work
SiC	3.2	82.77	204	[1]
c-BN	3.5	47.25	399	[1]
Hp-BN	3.6	34.02	382	This work
BP	2.8	93.45	171	[1]
b-Si_3N_4	3.2	145.46	236	[1]
AlN	3.3	81.86	197	[1]
BeS	2.4	115.5	113	[1]
BeSe	4.3	135.56	95	[1]
Al_2O_3	4.0	84.87	251	[1]
MgO	3.6	74.25	155	[1]
SiO_2	4.3	46.54	324	[1]
Os	19.1	33.11	421	This work
ReC	16.4	20.07	433	This work
OsC	16.6	20.28	406	This work
Re_2C	18.5	69.15	424	This work
ReOs	21.9	28.55	411	This work

Diamond*: the diamond upon charge injection of +0.25 e/atom.

Movie S1: Video of AIMD simulation of the diamond upon charge injection of –0.08 e/atom.

Movie S2: Video of AIMD simulation of the diamond upon charge injection of +0.25 e/atom.

Movie S3: Electron density redistribution for the diamond upon charge injection.

REFERENCE

1. Li, K.; Ding, Z.; Xue, D. Electronegativity-related bulk moduli of crystal materials. *Phys. Status. Solidi. (b)* **2011,** *248*, 1227-1236.